Electronic Supplementary Information

Ferroelectric bismuth-titanate nanoplatelets and nanowires with a new crystal structure

D. Makovec,* N. Križaj, A. Meden, G. Dražić, H. Uršič, R. Kostanjšek, M. Šala and S. Gyergyek

Materials

Bismuth(III) nitrate pentahydrate ($Bi(NO_3)_3 \cdot 5H_2O$, Alfa Aesar), tetra-n-butyl orthotitanate (Sigma-Aldrich), sodium hydroxide (NaOH, Sigma-Aldrich), nitric acid (HNO_3, Alfa Aesar), tert-butanol (EMSURE ACS).

Characterization

For the transmission (TEM) and scanning-transmission (STEM) electron microscopy studies, the nanoparticles were suspended in ethanol and deposited on a copper-grid-supported lacy carbon foil. For imaging along the nanowire, the nanowires were incorporated into poly(methyl methacrylate) (PMMA). To 5 g of MMA, 0.05 g of azobisisobutyronitrile (AIBN) initiator was added. The solution was poured into a glass vial, closed and heated to 80 °C in a dryer. The polymerization mixture was cooled to room temperature when it reached the consistency of honey. Then the nanowires were mixed in and dispersed by sonication for 10 minutes. The mixture was set hard by heating to 80 °C for 30 min. The composite in the form of a cylinder was cut in half. Then, from the inner section of the composite thin slices were cut with ultramicrotome Leica Reichert Ultracut S.

The TEM analyses were performed using a field-emission electron-source TEM Jeol 2010F operated at 200 kV. Quantitative analyses were performed using an energy-dispersive x-ray spectroscopy (EDXS) microanalysis system (LINK ISIS EDS 300) and Oxford ISIS software containing a library of virtual standards. Because bismuth evaporated/migrated from the nanoparticles under the intense electron beam, the spectra for quantification were collected with a beam spread over an area of specimen containing several tens of nanoparticles.

For the STEM analyses a -Csprobe -corrected Jeol ARM 200CF STEM was operated at 80 kV. During positioning and tilting of the nanoparticles in TEM mode a minimal intensity of beam was used to limit the degradation of the specimen under the beam. During the STEM imaging, HAADF and ABF detectors were used simultaneously at 68–180 and 10–16 mrad collection semi angles, respectively. To minimize the specimen drift, images were taken several hours after the insertion of the sample into the microscope and at least 20 minutes after the last sample positioning to minimize the goniometer drift.

X-ray powder diffraction data were collected in the reflection geometry using a PANalytical X'Pert Pro MPD powder diffractometer operating at 45 kV and 40 mA, using Cu-$K_{\alpha 1}$ radiation (λ = 1.5406 Å) in the range between 5 and 105 °2θ in a continuous mode. The full range of a 128-channel multi-strip solid-state linear position-sensitive detector was used to integrate intensities in steps of 0.33 °2θ and the effective measuring time per step of 2400 s.

A LeBail profile fit was performed using Topas Academic software V 7.0 x1.[S1] Anisotropic peak broadening was applied to account for significantly narrower peaks of the h 0 0 reflections.

Raman spectra of the samples were recorded with a NT-MDT model Integra Spectra for Materials Science equipped with a confocal microscope (20× magnification) at room temperature. A 633-nm laser diode was used for the excitation. The scattered light was detected using a cooled CCD camera and a 600 grooves/mm grating, and 10 spectra were accumulated, each acquired for 60 s to increase the signal-to-noise ratios.

Chemical composition of the nanoparticles (content of Bi, Ti, and Na) was measured with inductively coupled plasma (ICP-OES) using a Varian 715-ES ICP optical emission spectrometer. Prior to ICP-OES analysis, the lithium metaborate fusion digestion was used. Shortly, approximately 25 mg of sample was weighted and 500 mg of fused, anhydrous lithium tetraborate with lithium metaborate and lithium bromide (66.67% $Li_2B_4O_7$, 32.83% $LiBO_2$, 0.5% LiBr, Claisse, Canada) was added in Pt-beakers. These were then melted with a burner, allowed to cool, and subsequently leached in 40 ml of 25% v/v HNO_3. The resulting solutions were then diluted to obtain the desired concentration range for the constructed calibration curve. For sample dilution and the preparation of standards, ultrapure water (18.2 MΩ cm^{-1}, Milli-Q, Millipore) and ultrapure acid (HNO_3, Merck-Suprapur) were used. Standards were prepared in-house by dilution of certified, traceable, ICP-grade single-element standards (Merck CertiPUR). The relative standard deviation of the measurements was below 2 %.

For piezoresponse force microscopy (PFM) the sample powders were fixed with epoxy resin to prevent the nanoparticles from sticking to the PFM tip. This was done in the following manner. The mixture of EpoFix Liquid (Struers, Denmark) and EpoFix Powder (Struers, Denmark) was poured into the model containing the sample powder. After hardening, the epoxy/nanoparticles composite was removed from the model, ground and polished with SiC and a diamond paste, and finely polished with a colloidal silica suspension (Struers, Denmark) for 1.5 h. The topography and the piezo-response force microscope images were scanned using an atomic force microscope (AFM; Jupiter XR, Asylum Research, CA). A Pt-coated Si tip (OMCL-AC240TM-R3, Olympus, Japan) with a radius of curvature of ~15 nm was used. The electric field was applied to the thick film/epoxy resin composite in the virtual ground regime as previously described in ref. S2. PFM images were obtained in vector PFM mode at 2 V / 8 V and ~300 kHz (vertical) and 22 V / 75 V and ~700 kHz (lateral).

LeBail profile fitting of the X-ray powder diffraction pattern of BIT nanowires

LeBail profile fitting of the NW XRD pattern gave a satisfactory profile fit (Fig. SI1, R_{wp} = 4.76 %) and confirmed the orthorhombic unit cell.

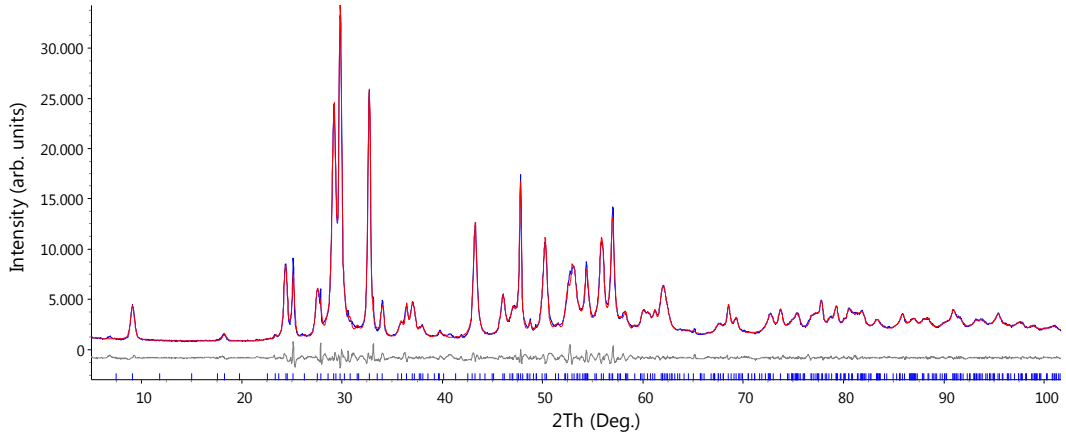

Fig. SI1 LeBail profile fit of X-ray powder diffraction pattern of BIT nanowires. The blue line is the measured pattern, red is calculated, grey in the middle is the difference and the blue vertical bars at the bottom denote reflection positions.

Raman spectroscopy

Our analysis of Raman spectra (Fig. SI2) focused on internal vibrational modes of TiO_6 octahedron. These bands are marked according to established nomenclature (Fig. SI1).[S3] The most important finding is that bands ν_4 (combination of stretching and bending vibrations)[S3] and $\nu_{5,6}$ (internal angle bending vibration - Raman active only in distorted octahedron)[S3] for the NPLs are found at lower Raman shifts than for the NWs. A similar shift is found for the TiO_2 polymorphs anatase and rutile. The TiO_6 octahedron vibrations are found at lower Raman shifts for the rutile phase where TiO_6 octahedra share corners and edges, as opposed to anatase, where octahedra share edges only.[S4] By the same analogy we conclude that the difference in the position of the bands in NPLs and NWs can be related to the different connectivity of the TiO_6 octahedra, being edge sharing in the case of NWs and corner sharing in the case of NPLs.

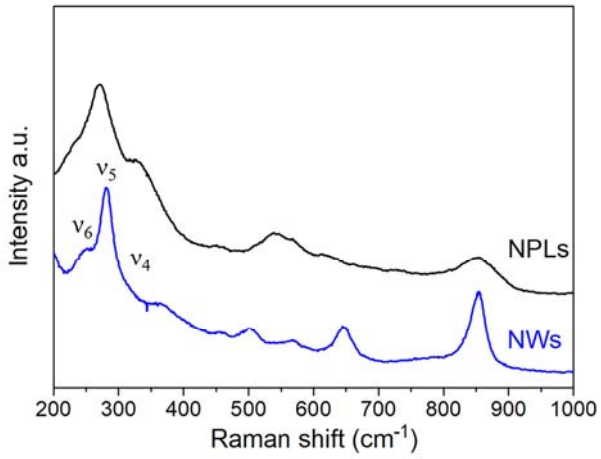

Fig. SI2 Raman spectra of NWs and NPLs.

Annealing of nanowires

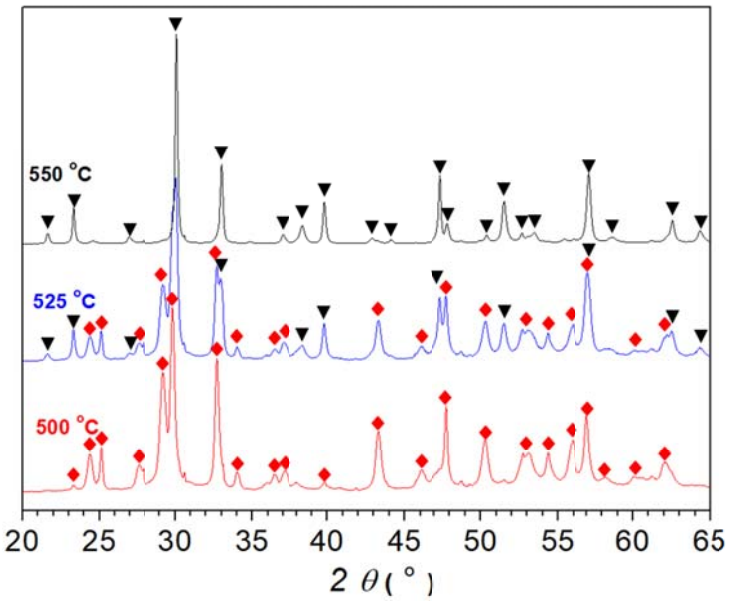

Fig. SI3 XRD of nanowires annealed for 2 hours at 500 ^{o}C, 525 ^{o}C and 550 ^{o}C.

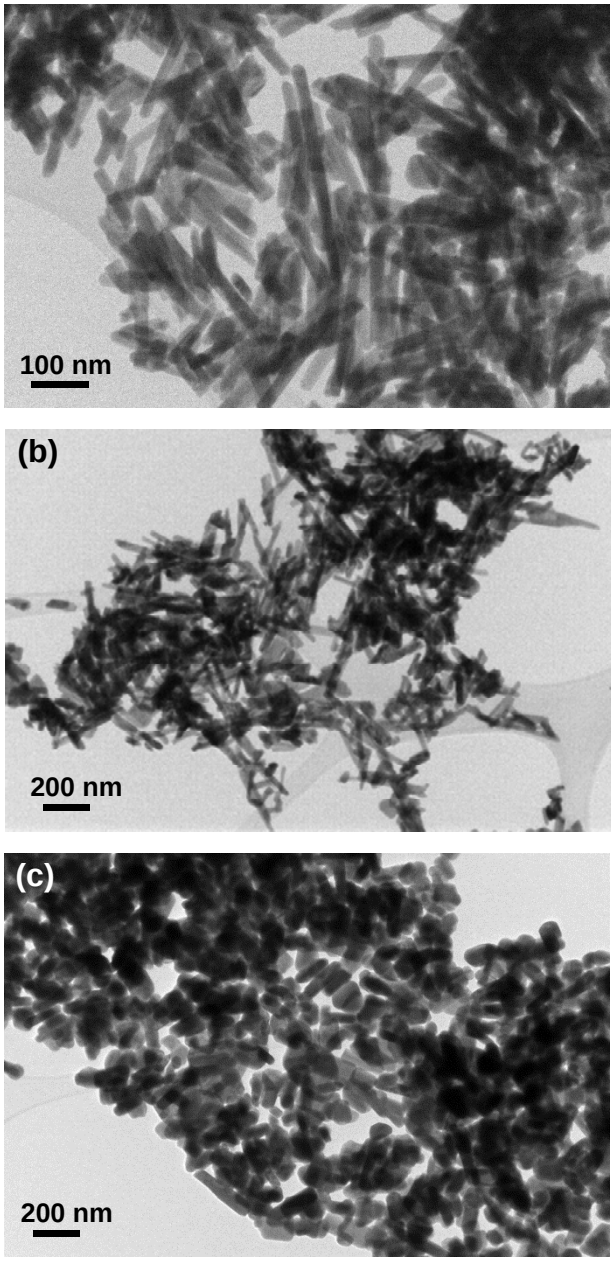

Fig. SI4 TEM of nanowires annealed for 2 hours at 500 ^{o}C (a), 525 ^{o}C (b) and 550 ^{o}C (c).

Observation of domain structure in NPLs

Fig. SI5(b) shows an atomic-resolution HAADF STEM image of NPLs oriented along [001] of its monoclinic $P1a1$ cell. The corresponding FFT patterns were calculated for the whole image (FFT pattern (e)) and, separately, for the left area of the image (a) (area marked with a red rectangle "A", FFT pattern (c)) and right area of the image (a) (area marked with a rectangle "B", FFT pattern (d)). The position of the $(010)_{AU}$ reflection in the FFT patterns suggests that the polarization directions in the two areas are oriented orthogonal (the direction of polarization vector ***P*** is illustrated with red arrows). In the monoclinic BIT the main component of the polarization lies along the a-axis.[S5]

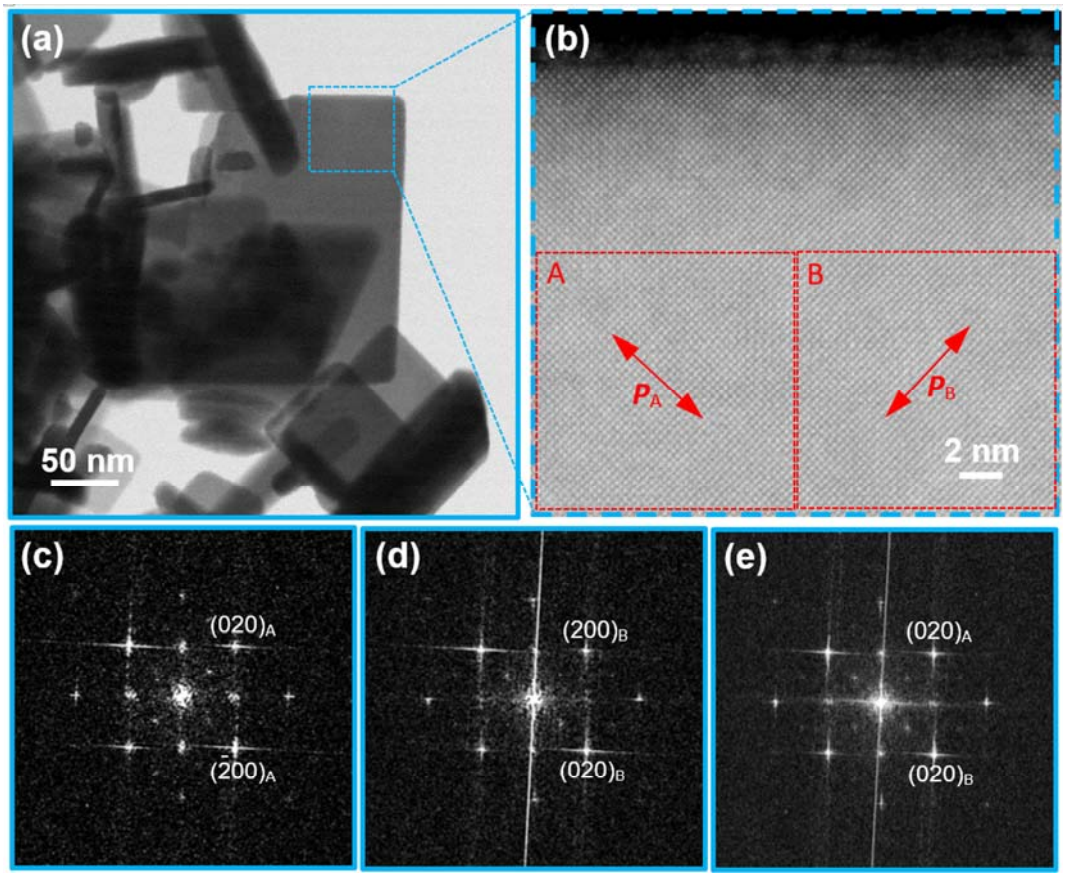

Fig. SI5 HAADF STEM image of a small NPL oriented along $[001]_A$ with FFT images of the areas of the NPL marked with red rectangles A and B.

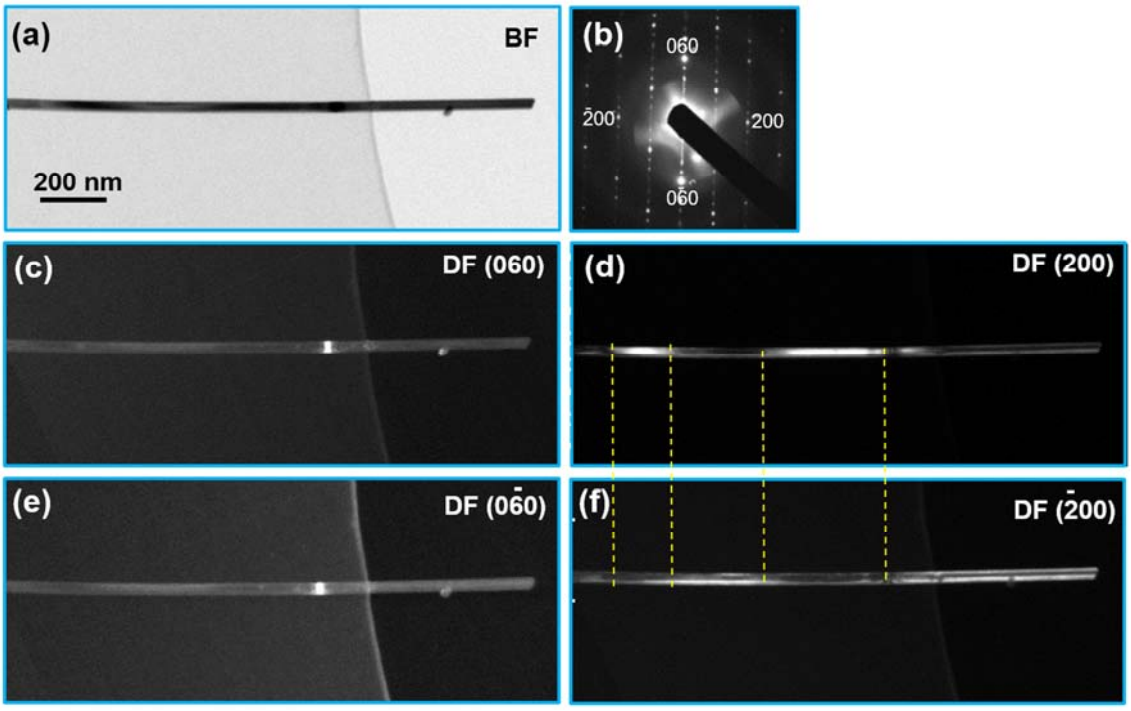

Fig. SI6 BF TEM image of a NW oriented along $[001]_{NW}$ direction (a) with corresponding electron diffraction pattern (b) and DF images formed with (060) (c) (200) (d), (0-60) (e), and (-200) (f) reflections. Dashed lines mark approximate positions of domain boundaries.

Switching and inducing ferroelectric domains in NPLs

PFM amplitude and phase images of nanoplates embedded in plastic were acquired in lateral dual-AC resonance tracking mode (lateral DART) at an AC amplitude signal of 15 V and ~740 kHz. Ferroelectric domains can be seen in the PFM in-plane amplitude and phase images of the single plate (Figs. SI7(c) and (d)). The domain boundaries can be identified in the amplitude image as non-active (dark) regions within the plate.

The PFM amplitude and phase hysteresis loops were measured in lateral switching spectroscopy (SS) off-electric field mode with the pulsed DC step signal and the superimposed AC drive signal, as explained in [ref. S1]. The waveform parameters were as follows: the sequence of rising steps of the DC electric field was driven at 10 Hz and a maximum amplitude of 75 V; the frequency of the triangular envelope was 0.99 Hz; an overlapping sinusoidal AC signal with an amplitude of 25 V and a frequency of ~740 kHz was used. Three cycles were measured in an off-electric field mode. The in-plane local PFM amplitude and phase hysteresis loops typical of piezoelectric/ferroelectric materials are shown in Figs. SI7(e) and (f).

After the SS experiment, the PFM in-plane amplitude and phase images were again acquired in the lateral DART mode at an AC amplitude signal of 10 V and ~740 kHz. Newly induced ferroelectric domains are observed in the region where the SS experiment was performed (marked with dashed blue rectangles in Figs. SI7(g) and (h)).

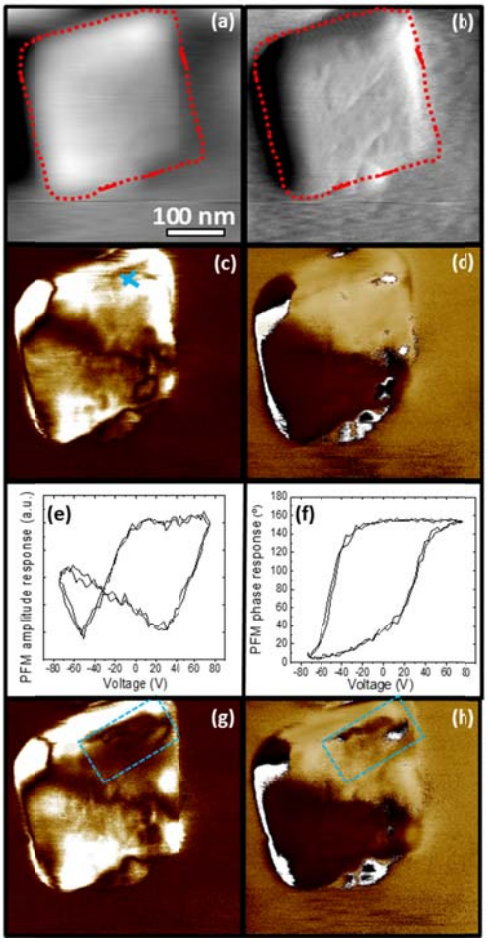

Fig. SI7 AFM (a) height and (b) deflection images, PFM (c) in-plane amplitude and (d) phase images. SS experiment, the local hysteresis loops of the PFM in-plane (e) amplitude and (f) phase measured at the point marked by crosses in panel (c). The second and third cycles are shown. PFM in-plane (g) amplitude and (h) phase images scanned after the SS experiment. The region where the induced ferroelectric domains are observed is highlighted in panels (g) and (h) by dashed blue rectangles.

References

S1. H. Uršič, U. Prah, Investigations of ferroelectric polycrystalline bulks and thick films using piezoresponse force microscopy, Proc. R. Soc. A, 475 (2223) (2019) 20180782-1 - 20180782-25.

S2. S.A.A. Coelho, TOPAS & TOPAS-Academic: An optimization program integrating computer algebra and crystallographic objects written in c++, J. Appl. Cryst., 51 (1) (2018) 210-218.

S3. S. Kojima, R. Imaizumi, S. Hamazaki, M. Takashige, Raman scattering study of Bismuth layer-structure ferroelectrics, Jpn. J. Appl. Phys., 33 (1) (1994) 5559-5564.

S4. U. Balachandran, N.G. Eror, Raman spectra of titanium dioxide, J. Solid State Chem., 42 (3) (1982) 276-282.

S5. D. Urushihara, M. Komabuchi, N. Ishizawa, M. Iwata, K. Fukuda, T. Asaka, Direct observation of the ferroelectric polarization in the layered perovskite Bi4Ti3O12, J. Appl. Phys. 120 (14) (2016) 142117-1 - 142117-5.